Arabian Journal of Chemical and Environmental Research

Vol. 06 Issue 2 (2019) 112–125

Computational POM and 3D-QSAR evaluation HIV-1-Integrase inhibition of β-amino Dicarbonyl Ligands

I. El Meskini [a], M H. Youssoufi [b], S. Shityakov [c], L. Toupet [d], M. Daoudi [a], A. Kerbal [a], Z. Hakkou [e], A. Lamhamdi [f], K. Azzaoui [g,*]

[a] *Laboratoire de Chimie Organique, Faculté des Sciences Dhar Mehraz, 30000 Fès, Maroc.*
[b] *Laboratory of ACE, Faculty of Sciences, Department of Chemistry. Mohammed First University, 60000 Oujda, Morocco*
[c] *Department of Bioinformatics, Würzburg. University, 97074 Würzburg, Germany; orcid.org/0000- 0002-6953-9771*
[d] *Institut de Physique - IPR - UMR CNRS 6251, Université de Rennes 1, Rennes, France.*
[e] *Laboratoire de Physiologie et Ethnopharmacologie URAC40, Faculté des Sciences, Université Mohammed Premier, Oujda, Morocco*
[f] *Laboratory of ASNSAS d'Al-hoceima. BP 03, Ajdir. Abdelmalek Essaadi University, Morocco*
[g] *Laboratory of LMSAC, Department of Chemistry, Faculty of Sciences, Mohamed 1st University, P.O. Box 717, Oujda 60000, Morocco*

Received 18 Dec 2019, Revised 26 Dec 2019, Accepted 26 Jan 2020

Abstract

A computational model has been created for the judicious plan of bioactive pharmacophore destinations as antiviral up-and-comers dependent on the accessible X-beam structure. The compound has been screened before antiviral action against HIV integrase (HIV IN). Amongst the series, the most potent compounds, 13 and 14 were tested in viral cultures for their ability to present potentials for anti-viral pharmacophore site and represent a low risk of toxicity. In addition, compounds 13 and 14 show potent anti-HIV IN activity. A good correlation was obtained between the theoretical predictions of bioavailability using POM suite (Petra/Osiris/Molinspiration containing Lipinski's rule-of-five) and experimental verification. The structure-activity relationship was also analyzed to prove the POM results.

Keywords: β-amino dicarbonyl compounds, Amide-containing diketoacids Virtual screening (POM), Anti-viral activity 3D-QSAR.

* Corresponding author. Khalil Azzaoui, Tel: +212 677042082
E-mail address: k.azzaoui@yahoo.com,

ISSN : 2458-6544

1. Introduction

We have developed a technology platform in cooperation with the United States NCI and TACF, which can easily access a diverse library based on antibacterial, antitumor and anti-HIV pharmacophore sites, and adopt this technology to discover potent viruses' inhibitors modelling the anti-bacterial/anti-fungal/ anti-viral pharmacophore sites [1]. There is considerable growing interest in these β-amino Dicarbonyl Ligands as anti-viral agents, exhibiting potentially similar pharmacophore pockets to that observed for ligands. Several groups Reported [2,6], failed attempts to obtain definite antiviral activity in these compounds, thus making people doubt the structural requirements. In order to better understand the inhibitory mechanism of HIV Integrase (HIV IN) [8], a series of anti-HIV were used Collected literature [9] and studied anti-HIV IN enzymes through molecular docking. We will exemplify the principle of POM technology by successfully discovering the effective antiviral activity against HIV virus in vitro and compare it with experimental data A comparison between experiment and theoretical predictions of the anti-viral activity has enabled us to identify alternative anti-viral structures. Results from all aspects of this bioinformatic approaches will be discussed.

For the preparation of such polydentate ligands, the aza-Michael reactions appear to be the key-step leading to the production of the β-amino esters [10]. In fact, this kind of reaction has been widely employed to generate structurally diverse β-amino dicarbonyl compounds, where the importance of the aza-Michael step can be seen from a large number of unconventional methodologies, as well as the broad range of applications [11]. Most of these unconventional methodologies have used Lewis acids, which, although leading to satisfactory yields, require to remove the Lewis acids [12]. Moreover, the use of an aqueous medium also has been successfully achieved [13]. Usually, these substrates are less reactive or conversely more resistant to undergo the Michael addition, resulting in the low conversion of the desired adducts [14]. From a synthetic point of view, this is a considerable limitation on the Michael reaction process and poses a significant challenge.

Results and discussion

1. Synthesis

The synthesis of various β-amino Dicarbonyl Ligands, introducing substituents on the terminal aryl ring (**Scheme 1**), and increasing the length of the carbon chain between the terminal benzene ring and the amide group, was previously reported in detail [5].

This efficient synthesis for a range of β-amino Dicarbonyl Ligands has been established. The flexibility of the synthesis could allow further development of a wide range of derivatives able to coordinate selectively with one or two transition metal centers.

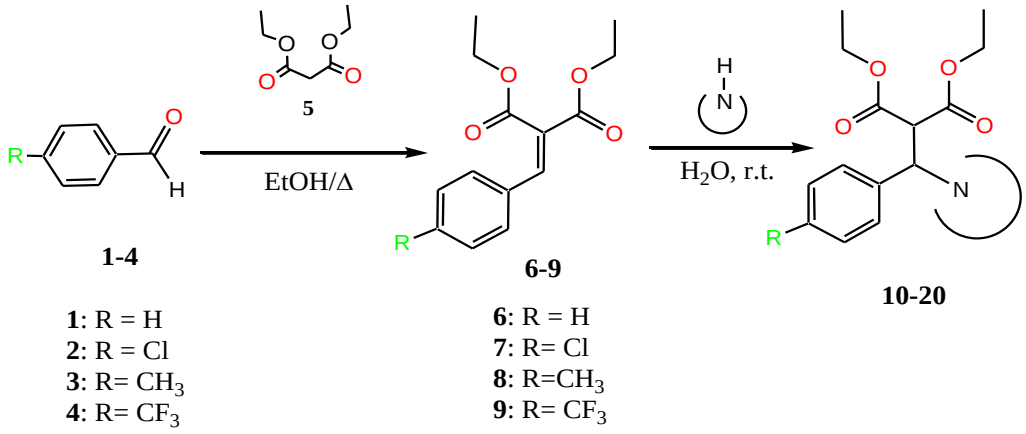

Scheme 1. Synthesis protocol of aminodicarbonyl compounds (**10-20**).

Table 1. Investigation of the aqueous medium-promoted aza-Michael condensation.

Entry	Starting materials [b]		Compd.	Experl data [a]	
	Amine	Malonate		Time	Yield %
1		**6**	**10**	12 h	71
2	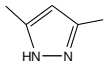	**8**	**11**	12 h	76
3		**9**	**12**	20 mn	73
4	$PhCH_2$-N-CH_2Ph H	**6**	**13**	4 h	76
5	$PhCH_2$-N-CH_2Ph H	**7**	**14**	12 h	67
6	$PhCH_2$-N-CH_3 H	**6**	**15**	4 h	78
7	$PhCH_2$-N-C_2H_5 H	**6**	**16**	8 h	82
8		**9**	**17**	10 mn	67
9		**8**	**18**	4 h	74
10		**9**	**19**	10 mn	96
11	$PhCH_2$-N-CH_2Ph H	**9**	**20**	10 mn	63

2. Computational Studies

2.1. Computational methods

In the context of this study, all stationary points involved in this nucleophilic addition reaction were optimized using the B3LYP functional together with the standard 6-31G(d) basis set. The stationary points were characterized by frequency computations in order to verify [15] that TSs have one and only one imaginary frequency. The IRC paths were traced in order to check the energy profiles connecting each TS to the two associated minima of the proposed mechanism using the second-order González–Schlegel integration method. Solvent effects of water were taken into account by single-point energy calculations using the conductor-like polarizable continuum model (CPCM) developed by Tomasi's group in the framework of the self-consistent reaction field (SCRF) [15]. The global electron density transfer (GEDT) [16] was computed by the sum of the natural atomic charges (q), obtained by a natural population analysis (NPA) [16], of the atoms belonging to each framework (f) at the TSs; GEDT = Σq_f. The sign indicates the direction of the electron density flux in such a manner that positive values mean a flux from the considered framework to the other one. All computations were carried out with the Gaussian 09 suite of programs.

The global electrophilicity index, ω, is given by the following expression, $\omega=(\mu^2/2\eta)$, in terms of the electronic chemical potential, μ, and the chemical hardness, η. Both quantities may be approached in terms of the one-electron energies of the frontier molecular orbitals HOMO and LUMO, ε_H and ε_L, as $\mu\approx(\varepsilon_H+\varepsilon_L)/2$ and $\eta=(\varepsilon_L-\varepsilon_H)$, respectively. The empirical (relative) nucleophilicity index[33.34] N, based on the HOMO energies obtained within the Kohn–Sham scheme[35], is defined as $N = E_{HOMO}(Nu) - E_{HOMO}(TCE)$, where tetracyanoethylene (TCE) is the reference, because it presents the lowest HOMO energy in a long series of molecules already investigated in the context of polar organic reactions. Besides the global electrophilicity index, it is possible to define its local (or regional) counterpart condensed to atoms. The local electrophilicity, ω_k, or local nucleophilicity N_k, condensed to atom k is easily obtained by projecting the global quantity onto any atomic center k in the molecule by using the Parr function. $\omega_k = \omega . P_k^+$ and $N_k = N . P_k^-$. The electrophilic, P_k^+, and nucleophilic, P_k^-, Parr functions, were obtained through the analysis of the Mulliken ASD of the radical anion and the radical cation by single-point energy calculations over the optimized neutral geometries using the unrestricted UB3LYP formalism for radical species.

2.2. POM Analyses of compounds

The POM theory can determine the type of degree points for pharmacodynamics [6]. POM must have become a the most famous recent method often used [7] to generate 2D models Identify and point out

the effects of antibacterial, antiviral and the antifungal activity changes with chemical substitution and partial charge distribution. In fact, the real advantage of POM theory is the ability to easily predict the biological activity of molecules and show the relationship between space / static properties and biological activity in the following form Pharmacodynamic degree points; this provides not only the key features of ligand-receptor interaction, but also the key features. The topology of the receptor coexists with tautomerism, isomerism and ring opening / closing Process.

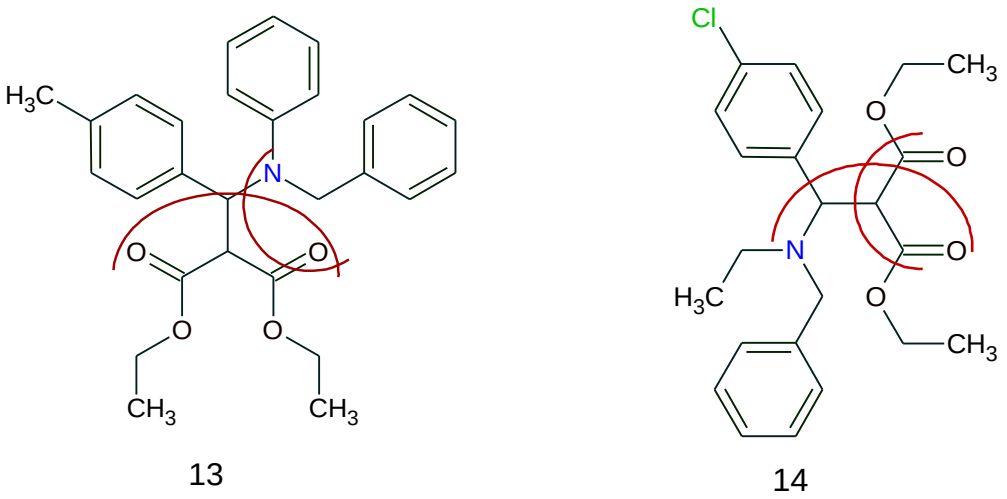

Scheme 2. Antiviral pharmacophore sites for 13 and 14

2.2.1. Osiris calculations

OSIRIS Property Explorer used in this study It is part of Actelion's internal substance registration system. It allows you to draw chemical structures and Real-time calculation of various drug-related properties as long as the structure is valid. Forecast results are valuable and coding. High-risk characteristics with adverse consequences If the mutagenicity or intestinal malabsorption is expressed as (-), and (+) Indicates that the drug meets Behavior (Table 2).

Table2. Osiris calculations of compounds.

Compd.	MW	ToxicityRisks[a]					Osiris calculations[b]			
		MUT	TUM	IRRI	REP		cLogP	cLogS	DL	DS
13	445						4.81	-4.95	-15.00	0.24
14	417						3.79	-3.80	-13.10	0.34

2.2.2. Molinspiration Calculations

Calculate the biological activity score (BS) of synthetic compounds with different parameters (such as TPSA, NH --- O or N-HO interaction and molecular volume) and compare it with some standard drugs Calculate all mentioned parameters with the help of Molinspiration online software

(www.molinspiration.com), which can predict the intermediate biological activity of synthetic compounds (L1-L11). As presented in Table 3.

Table 3. Molinspiration calculations of compounds.

Compd.	Molinspiration calculations						Drug-likeness					
	MW g/mol	cLogP	TPSA	OH--NH Interract.	N violation	Volume	GPCR ligand	ICM	KI	NRL	P I	EI
13	445.56	6.32	55.85	0	1	429.32	-0.23	-0.27	-0.35	-0.03	-0.23	-0.30
14	417.93	5.22	55.85	0	1	388.25	-0.04	-0.09	-0.40	-0.29	-0.17	-0.26

2.3. Molecular docking and molecular dynamics simulations

The integrase (IN) strand transfer inhibitors (INSTI) including BIC: bictegravir (BIC), dolutegravir (DOL), and elvitegravir (ELV) were designed *in silico* using the MarvinSketch v.14.7.14.0 software [8]. The consensus sequence representing the Cameroonian HIV-1 subtype CRF02_AG IN was generated using the CRF02_AG study sequences (n=37) as previously reported [9], accession number: MN816445-MN816488. The protein 3D structure was generated by using the SWISS-MODEL server, as a fully automated protein homology modeling work-flow. The AutoDock algorithm was implemented to perform the molecular docking with default settings. The binding site was determined according to the information obtained from the SIVrcm intasome bound to BIC (PDB ID: 6RWM) with Cartesian coordinates of 229.36 Å (x-axis), 226.86 Å (y-axis), and 191.68 Å (z-axis) [8]. The PyMOL molecular imaging software and the in-house Python data processing scripts were utilized to calculate the inhibition constants (*Ki*) from the $\Delta Gbind$ (Gibbs free energy of binding) values, generate high-quality graphics, and analyze the results (PyMOL Molecular Graphics System, Version 1.7.2.1, Schrödinger, LLC). The linear regression analysis was performed using the GraphPad Prism v.7 software for Windows.

Table 4. Binding affinities of analyzed compounds to HIV-1 IN

Compound	ΔG_{bind} (kcal/mol)	Ki (µM)	EC50 (nM)
BIC	-7.17	5.31	0.02*
DOL	-6.53	15.71	0.08*
14	-6.45	17.99	0.09
ELV	-6.21	21.01	0.11

*: Susceptibilities of HIV-1 IN to INSTI compounds in TZM-bl cells [7]

After *in silico* screening of N,O,O-ligands (n = 15, Scheme 1) to estimate their binding affinity to the HIV-1 IN protein, most of them were found to be non-binders ($\Delta G_{bind} > -6.0$ kcal/mol) except for compound 14 ($\Delta G_{bind} = -6.45$ kcal/mol). This hit compound represented the binding affinity to the

protein target comparable to the INSTI drugs (positive control), which was lower than for BIC and DOL but higher than that of ELV (Table 4, Figure 6). Finally, the linear relationship was determined with reliable statistics (R^2 = 0.99, P-value = 0.0006) between the experimental data as half-maximal effective concentrations (EC50) published elsewhere and predicted inhibition constants (Figure 7).

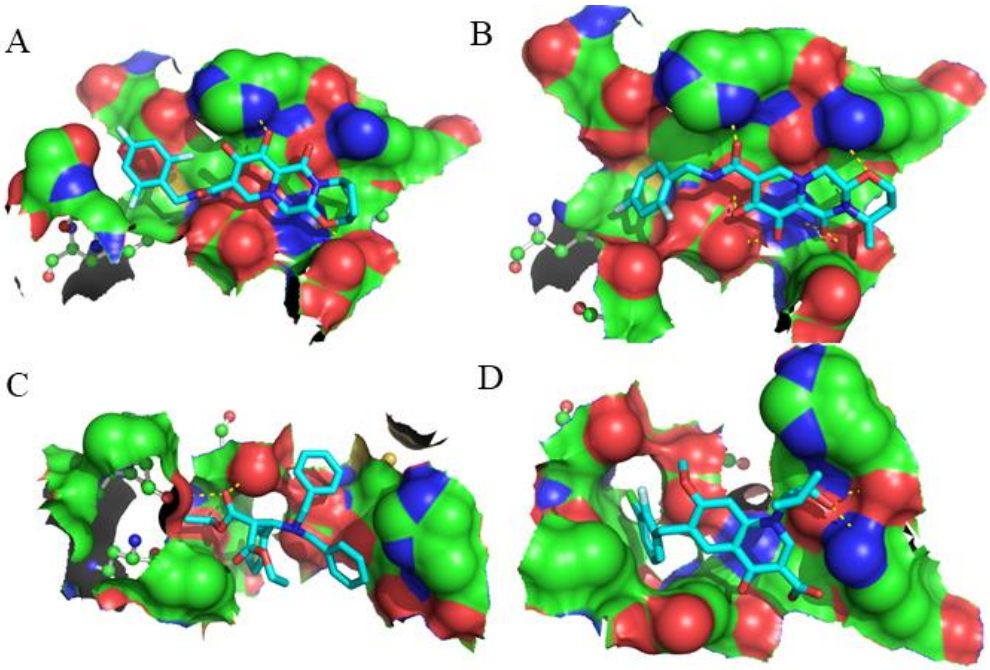

Fig 6. Binding conformations predicted from the AutoDock runs for BIC (A), DOL (B), ELV (C), and compound 14 (D) bound to HIV-1 IN. The protein binding site is shown by molecular surface and colored according to the protein atomic composition. All protein residues are drawn as ball-and-stick models. Hydrogen bonds are visualized as dashed lines. The ligand molecules are depicted in sticks and hydrogen atoms were removed to enhance clarity.

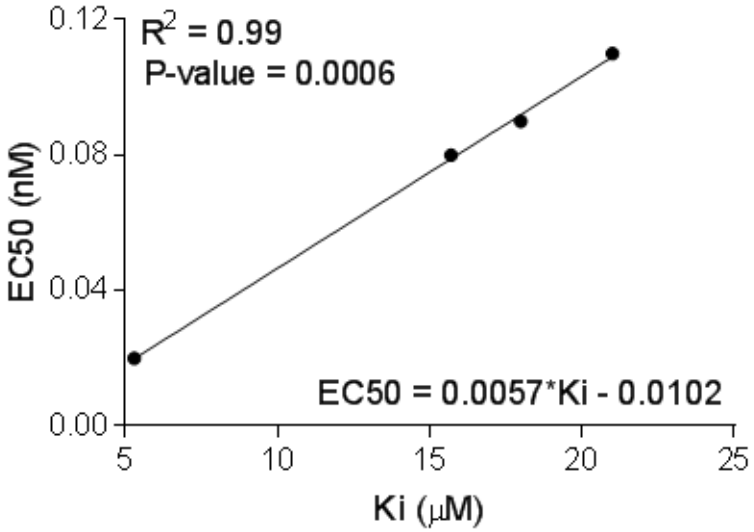

Fig 7. Linear relationship between the predicted binding constants calculated from the docking studies of INSTI with HIV-1 IN and the experimental EC50 values determined from the TZM-bl cells-based assay.

2.4.2 Quantum chemical study

In the context of this study, all stationary points involved in this nucleophilic addition reaction were optimized using the B3LYP functional together with the standard 6-31G(d) basis set. The stationary points were characterized by frequency computations in order to verify that TSs have one and only one imaginary frequency [21]. The IRC paths were traced in order to check the energy profiles connecting each TS to the two associated minima of the proposed mechanism using the second-order González–Schlegel integration method [22]. Solvent effects of water were taken into account by single-point energy calculations using the conductor-like polarizable continuum model (CPCM) developed by Tomasi's group in the framework of the self-consistent reaction field (SCRF). The global electron density transfer (GEDT) was computed by the sum of the natural atomic charges (q), obtained by a natural population analysis (NPA), of the atoms belonging to each framework (f) at the TSs; GEDT = Σq_f. The sign indicates the direction of the electron density flux in such a manner that positive values mean a flux from the considered framework to the other one. All computations were carried out with the Gaussian 09 suite of programs [23].

The global electrophilicity index, ω, is given by the following expression, $\omega=(\mu^2/2\eta)$, in terms of the electronic chemical potential, μ, and the chemical hardness, η. Both quantities may be approached in terms of the one-electron energies of the frontier molecular orbitals HOMO and LUMO, ε_H and ε_L, as $\mu\approx(\varepsilon_H+\varepsilon_L)/2$ and $\eta=(\varepsilon_L-\varepsilon_H)$, respectively. The empirical (relative) nucleophilicity index [22] N, based on the HOMO energies obtained within the Kohn–Sham scheme[35], is defined as $N = E_{HOMO}(Nu) - E_{HOMO}(TCE)$, where tetracyanoethylene (TCE) is the reference, because it presents the lowest HOMO energy in a long series of molecules already investigated in the context of polar organic reactions [23, 28]. Besides the global electrophilicity index, it is possible to define its local (or regional) counterpart condensed to atoms. The local electrophilicity, ω_k, or local nucleophilicity N_k, condensed to atom k is easily obtained by projecting the global quantity onto any atomic center k in the molecule by using the Par function. $\omega_k = \omega . P_k^+$ and $Nk = N . P_k^-$. The electrophilic, P_k^+, and nucleophilic, P_k^-, Parr functions, were obtained through the analysis of the Mulliken ASD of the radical anion and the radical cation by single-point energy calculations over the optimized neutral geometries using the unrestricted UB3LYP formalism for radical species [29]. Global and local electrophilicity/nucleophilicity index analysis. Studies on polar organic reactions have shown that the analysis of the reactivity indices defined within the conceptual DFT[36.37] (CDFT) is a powerful method to understand the reactivity in polar reactions. Consequently, the global CDFT indices, namely, the electronic chemical potential, μ, chemical hardness, η, electrophilicity, ω, and nucleophilicity, N, of the benzyl ethylamine and 2-(4-Chlorobenzylidene) ethyl malonate are given in Table 5.

Table 5. Electronic chemical potential (**μ**, in ev), chemical hardness (**η**, in ev), global ectrophilicity (**ω**, in eV) and global nucleophilicity N of amine and alkene.

	μ	**η**	**ω**	**N**
benzyl ethylamine	-2,87	6,03	0,68	3,22
2-(4-Chlorobenzylidene) ethylmalonate	-4,24	4,45	2,02	2,65

The electronic chemical potential of benzyl ethylamine, μ= -2.87 eV, is higher than that 2-(4-Chlorobenzylidene) ethylmalonate, μ= -4.4 eV, indicating that along with a polar reaction the GEDT[35] will flux from the benzyl ethylamine framework towards the 2-(4-Chlorobenzylidene) ethylmalonate one. In agreement with the GEDT computed at the TSs (see later) [30].

The benzyl ethylamine is a marginal electrophile ω = 0.68 eV, and a strong nucleophile N= 3.22 eV within the ω and N scal. 2-(4-Chlorobenzylidene) ethylmalonate has an electrophilicity ω index of 2.02 eV, is then classified as a strong electrophile, and a nucleophilicity index of 2.65 eV, is classified as a moderate nucleophile.

The high electrophilic character of 2-(4-Chlorobenzylidene) ethylmalonate and the high nucleophilic character of benzyl ethylamine make that alkene will act as the electrophile and amine as the nucleophile in this reaction with a large polar character [31].

Along with a polar reaction involving the participation of non-symmetric reagents, the most favorable reactive channel is that involving the initial two-center interaction between the most electrophilic center of the electrophile and the most nucleophilic center of the nucleophile. Recently, Domingo proposed the electrophilic P_k^+ and nucleophilic P_k^- Parr functions [32] as powerful tools in the study of the local reactivity in polar processes. Hence, in order to characterise the most nucleophilic and the most electrophilic centers of the species involved in this nucleophilic addition reaction, and, thus, to explain the regioselectivity experimentally observed, the electrophilic P_k^+ Parr functions of 2-(4-Chlorobenzylidene) ethylmalonate, and the nucleophilic P_k^- Parr functions of benzyl ethylamine were analysed (Scheme 3).

Analysis of the nucleophilic P_k^- Parr functions of benzyl ethylamine indicates that the amine N1 nitrogen, P_k^- = 0.44 (N_{N1} = 1.44 eV) is the most nucleophilic center of this species. On the other hand, analysis of the electrophilic P_k^+ Parr functions of 2-(4-Chlorobenzylidene) ethylmalonate indicates that the C1 carbon, P_k^+ = 0.31 (ω_{C1} = 0.62 eV) is also the most electrophilic center [33]. Consequently, the most favorable nucleophilic/electrophilic two centers interaction along C-N single bond formation will take place between the N1 nitrogen atom of amine and the C1 carbon atom of an alkene, in clear agreement with the regioselectivity experimentally observed,

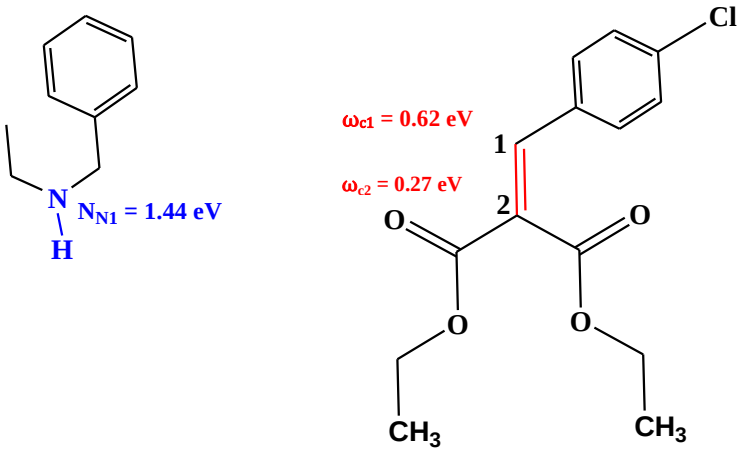

Scheme 3. Locale electrophilicity ω_k of 2-(4-Chlorobenzylidene) ethylmalonate in red, and the locale nucleophilicity N_k of benzyl ethylamine in blue.

Analysis of the stationary points involved in the reaction between 2-(4-Chlorobenzylidene) ethylmalonate and benzyl ethylamine indicates that this nucleophilic addition reaction takes place through a stepwise mechanism, two TSs, TS1 and TS2, and one intermediate, IN, have been located and characterized (Figure 4). In the first step of this mechanism is a nucleophilic attack to the carbon atom of alkene *via* the nitrogen atom of amine, forming an intermediate, **IN.** The calculated barrier is 8.97 kcal mol^{-1}. Whereas the formation of the zwitterionic intermediate **IN** is located 2.27 kcal/mol below than TS1. The second step, the C2 carbon of the alkene in **IN** rips off the ammonium proton, forming the corresponding product [34]. The calculated barrier is 33.70 kcal mol^{-1}. This step corresponds to the rate-determining step of the stepwise process.

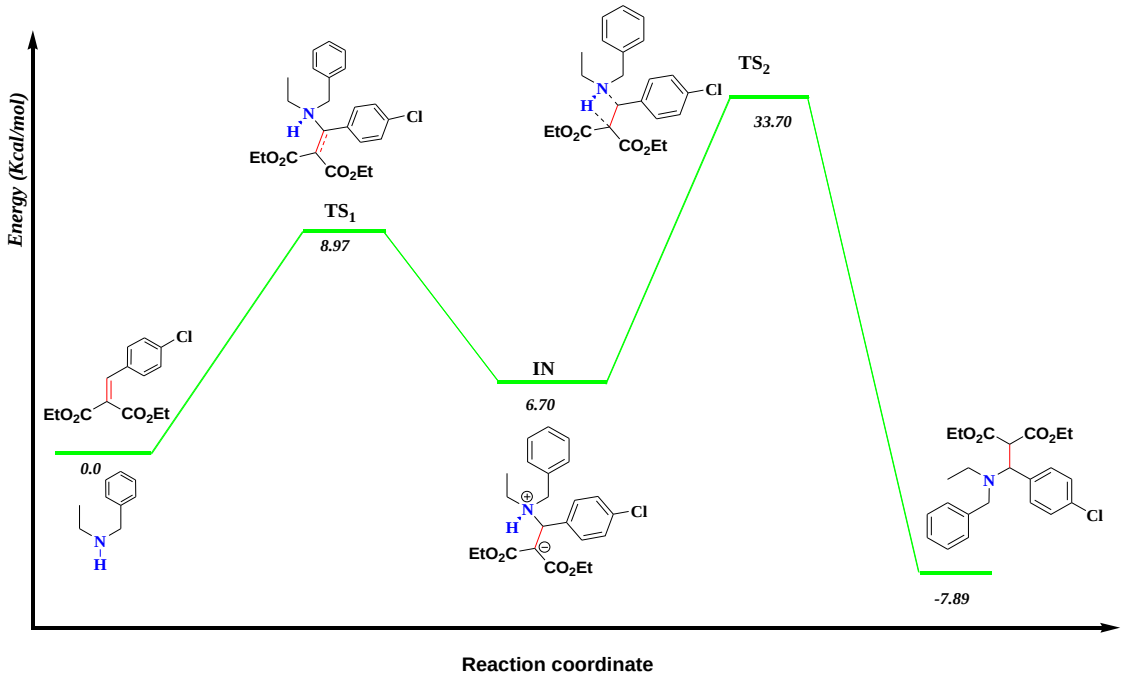

Fig 4. Schematic representation (energy vs reaction coordinate) of the nucleophilic addition reaction between benzylethylamine and 2-(4-Chlorobenzylidene) ethylmalonate

The geometries of the TSs associated to the nucleophilic addition reactions between 2-(4-Chlorobenzylidene) ethylmalonate and benzyl ethylamine are given in Figure 4. The lengths of the C–N forming bonds at the TSs are: 1.846 (C1–N) Å at TS1 and 1.562 (C1–N), 1.333 (N–H) and 1.457 (C2–H) Å at TS2.

Numerous studies have shown a strong relationship between the polar character and the feasibility of organic reactions; the larger the GEDT at the TS is, the more polar and thus, faster, the reaction [35, 37]. In order to evaluate the electronic nature, i.e. polar or non-polar of the nucleophilic addition reaction between 2-(4-Chlorobenzylidene) ethyl malonate and benzyl ethylamine, the GEDT at the TSs was analyzed. The resulting values are reported in Figure 5. The natural charges at the TSs appear to be shared between the 2-(4-Chlorobenzylidene) ethylmalonate and benzyl ethylamine. The GEDT, which fluxes from amine to alkene at the TSs, is 0.45e at TS1 and 0.44e at TS2. These very high values indicate that these TSs have a polar character, in agreement with the high electrophilic character of 2-(4-Chlorobenzylidene) ethylmalonate and the high nucleophilic character of benzyl ethylamine.

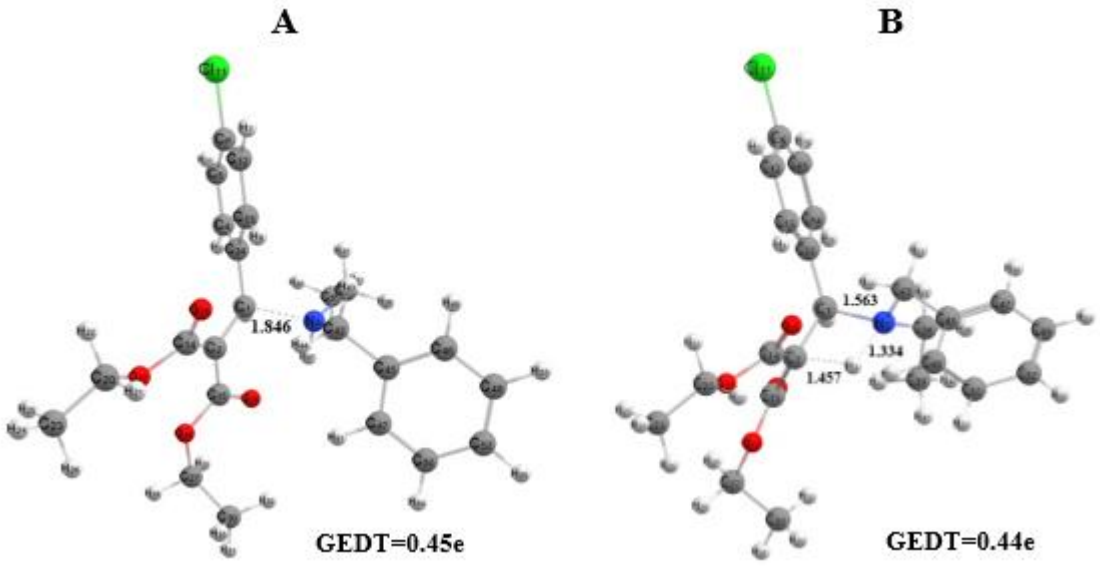

Fig 5. Optimized geometries of the TSs, TS1, and TS2, associated with nucleophilic addition reaction of 2-(4-Chlorobenzylidene) ethylmalonate benzyl ethylamine. The distances are **given in Å.**

Conclusion

These β-amino Dicarbonyl Ligands, typically could form the highly stable combined pharmacophore sites [O=C, C=C]. This structure allows us to program effective therapeutic drug candidates so that they have excellent chemical stability in terms of coordination chemistry and antiviral activity. Some active spiro-series tested previously, as anti-HIV agents are in the same desirable geometry. A number of important points emerge concerning the electronic and steric factors which have direct impact on

antiviral properties. The encouraging results we have recorded for the purposes of new drug designing, confirm that most of these compounds could be used for potential anti-viral activity after minor modifications. Based on their structural properties, these compounds could also be useful agents with potential activity. These results prompt several pertinent observations: (i) These types of DKAs can furnish an interesting model for studying the interaction of anti-biotics with viral targets because of the possible charge modification of substituents of pharmacophore group; (ii) The future rigid geometric conformation of pharmacophore site(s) enables us to prepare molecules for multi-therapeutic materials with high selectivity.

Conflict of Interest

The authors declare that the research was conducted in the absence of any commercial or financial relationships that could be construed as a potential conflict of interest.

References

[1] Z.H. Chohan, M.H. Youssoufi, A. Jarrahpour, T. Ben Hadda. Identification of antibacterial and antifungal pharmacophore sites for potent bacteria and fungi inhibition: indolenyl sulfonamide derivatives, *Eur J Med Chem*., 45 (3): 1189-1199 (2010). doi:10.1016/j.ejmech.2009.11.029

[2] A. Parvez, J. Meshram, V. Tiwari, Pharmacophores modeling in terms of prediction of theoretical physico-chemical properties and verification by experimental correlations of novel coumarin derivatives produced via Betti's protocol, *Eur J Med Chem*., 45 (9): 4370-4378 (2010). doi:10.1016/j.ejmech.2010.06.004

[3] M. Rbaa, S. Jabli, Y. Lakhrissi. Synthesis, antibacterial properties and bioinformatics computational analyses of novel 8-hydroxyquinoline derivatives. *Heliyon*, 5 (10): 2689 (2019). doi:10.1016/j.heliyon.2019.e02689

[4] K. Kailas. Synthesis and Characterization of 3-Amino Carbonyl Ligand by Infrared Spectroscopy. *Researchers world international referred research journal*., 7: 70-73 (2016).

[5] I. Meskini, T. Loïc, M. Daoudi, A. Kerbal, B. Bennani, P.H. Dixneuf, Z.H. Chohan, A. Leite, L. Cristina, T. Ben Hadda. An efficient protocol for accessing β-amino dicarbonyl compounds through aza-Michael reaction, *Journal of the Brazilian Chemical Society*, 21(6): 1129-1135 (2010). https://doi.org/10.1590/S0103-50532010000600025

[6] DT. Mahajan, VH. Masand, KN. Patil. CoMSIA and POM analyses of anti-malarial activity of synthetic prodiginines. *Bioorg Med Chem Lett*., 22 (14): 4827-4835 (2012). doi:10.1016/j.bmcl.2012.05.115

[7] ER. Elsharkawy, F. Almalki, T. Ben Hadda, V. Rastija, H. Lafridi, H. Zgou. DFT calculations and

POM analyses of cytotoxicity of some flavonoids from aerial parts of Cupressus sempervirens: Docking and identification of pharmacophore sites. *Bioorg Chem*., 100 10: 3 850 (2020). doi:10.1016/j.bioorg.2020.103850

[8] SA. Hassounah, A. Alikhani, M. Oliveira, S. Bharaj, R-I. Ibanescu, N. Osman. Antiviral Activity of Bictegravir and Cabotegravir against Integrase Inhibitor-Resistant SIVmac239 and HIV-1. *Antimicrob Agents Chemother*., 61 (12): (2017).

[9] G. Pirok, N. Mate, J. Varga, J. Szegezdi, M. Vargyas, S. V. Making "real" molecules in virtual space. *J Chem Inf Model*., 46 (2): 563-8 (2006).

[9] Y. Hayashi, J. J. Rode, E. J. J. Corey, *Am. Chem. Soc*., 118: 5502–5503 (1996).

[10] (a) P. H. Phua, S. P. Mathew, A. J. P. White, J. G. de Vries, D. G. Blackmond, K. K. M. *Hii, Chem. Eur. J.*, 13 4602–4613 2007); (b) Q. Zhu, H. Jiang, J. Li, M. Zhang, M. Wang, C. Qic, *Tetrahedron*, 65 (2009)

[11] (c) P. H. Phua, J. G. de Vries, K. K. Hii, Adv. Synth. Catal., 347 1775–1780 (2005); (d) S. Azad, T. Kobayashi, K. Nakano, Y. Ichikawa, H. Kotsuki, *Tetrahedron Lett*., 50 48-50 (2009); (e) D. Kumar, G. Patel, B. G. Mishra, R. S. Varma, *Tetrahedron Lett*., 49 6974-6976 (2008).

[12] (a) T. P. Loh, L. L. Wei, *Synlett*, 975–976 (1998), (b) B. Basu, P. Das, I. Hossain, *Synlett*., 2630–2632 (2004); (c) T. C. Wabnitz, J. B. Spencer, *Tetrahedron Lett*., 43 3891–3894 (2002); (d) M. K. Chaudhuri, S. Hussain, M. L. Kantam, B. Neelima, *Tetrahedron Lett*., 48 141-143 (2007); (e) B. C. Ranu, S. S. Dey, A. Hajra., *Arkivoc*, 7 76–81 (2002).

[13] (a) B. C. Ranu, S. Banerjee, *Tetrahedron Lett.* 2009, 50: 48-50; (b) Ranu, B. C.; Mandal T. *Synthetic Commun.* 2007, 37, 1517-1523; (c) B. C. Ranu, S. S. Dey, S. Samanta, *Arkivoc* 3: 44-50. 2005,

[14] D. Brado, A. E. Obasa, G. M. Ikomey, R. Cloete, K. Singh, S. Engelbrecht, U. Neogi, G. B. Jacobs, Analyses of HIV-1 Integrase Sequences Prior to South African National HIV-Treatment Program and Availability of Integrase Inhibitors in Cape Town, *South Africa. Sci Rep.*, 8 (1): 4709 (2018).

[15] T. Schwede, J. Kopp, N. Guex, MC. Peitsch. Swiss-Model: An automated protein homology-modeling server. *Nucleic Acids Res*., 31 (13): 3381-5 (2003).

[16] DS. Goodsell, GM. Morris, AJ. V. Automated docking of flexible ligands: Applications of AutoDock. *J Mol Recognit*. 9(1): 1-5 (1996).

[17] NJ. Cook, W. Li, D. Berta, M. Badaoui, A. V, A, Nans. Structural basis of second-generation HIV integrase inhibitor action and viral resistance. *Science*., 367 (6479): 806-10 (2020).

[21] B. Y. Simkin, I. Sheikhet, Quantum chemical and statistical theory of solutions computational approach. *Ellis Horwood, London*. (1995).

[22] E. Cances, B. Mennucci, J. Tomasi, *J. Chem. Phys*., 107 : 3032–3041 (1997).

[23] V. Barone, M. Cossi, J. Tomasi, Geometry optimization of molecular structures in solution by the polarizable continuum model. *J. Comput. Chem*., 19: 404–417 (1998).

[24] L. R. Domingo, Experimental and Theoretical MEDT Study of the Thermal [3+2] Cycloaddition Reactions of Aryl Azides with Alkyne Derivatives. *Chemistry Select*, 3: 1215– 1223 (2018).

[25] H. Ben El Ayouchia, B. Lahoucine, H. Anane, L. R. Domingo, and S-E Stiriba, *RSC Adv*., 8 76- 70 (2018).

[26] (a) A. E. Reed, R.B. Weinstock and F. Weinhold, *J. Chem. Phys.*, 83 735 (1985); (b) A. E. Reed, L.A. Curtiss and F. Weinhold, *Chem. Rev.*, 88: 899 (1988).

[27] M. J. Frisch et al., GAUSSIAN 09, Revision E. 01, Gaussian Inc, *Wallingford CT.*, (2009).

[28] RG. V, L. von Szentpaly, S. Liu, *J. Am. Chem. Soc*., 121: 1922–1924 (1999)

[29] RG. Parr, RG. Pearson, *J. Am. Chem. Soc*., 105: 7512–7514 (1983)

[30] RG. Parr, W. Yang, Density functional theory of atoms and molecules. *Oxford University Press, New York.*, (1989)

[31] LR. Domingo, E. Chamorro, P. Pérez , Understanding the reactivity of captodative ethylenes in polar cycloaddition reactions. A theoretical study. *J. Org. Chem*., 73: 4615–4624 (2008)

[32] LR. Domingo, P. Pérez. The nucleophilicity N index in organic chemistry. *Org Biomol Chem*., 9: 7168–7175 (2011)

[33] W. Kohn, L. Sham, Conceptual Density Functional Theory. *J Phys Rev* 140: 1133–1138 (1965).

[34] P. Geerlings, F. De Proft, W. Langenaeker, Absolute hardness: companion parameter to absolute electronegativity.*Chem. Rev.*, 103: 1793-1874 (2003).

[35] LR; Domingo, M; Ríos-Gutérrez, P; Pérez, Applications of the Conceptual Density Functional Theory Indices to Organic Chemistry. Reactivity, *Molecules.* 21: 748 (2016).

[36] P. Pérez, L.R. Domingo; M.J. Aurell; R. Contreras. The electrophilicity index in organic chemistry. *Terrahedron*., 59: 3117 (2003).

[37] L. R. Domingo, A new C–C bond formation model based on the quantum chemical topology of electron density. *RSC Adv*., 4: 32415 (2014).